Electronic Supplementary Information

Optical Writing and Single Molecule Reading of Photoactivatable and Silver Nanoparticle-Enhanced Fluorescence

Nicholas P. Dogantzis,[†][a] Gregory K. Hodgson[†][a] and Stefania Impellizzeri[*][a]

[a]Department of Chemistry and Biology, Ryerson University, 350 Victoria Street, Toronto, ON M5B 2K3, Canada
Corresponding Email: simpellizzeri@ryerson.ca

[†]These authors made equal contributions to this work

Content

Materials and Synthesis

N,N'-Difluoroboryl-5-(phenyl)dipyrrin: To a cleaned and oven-dried 500 mL round bottom flask equipped with a magnetic stir bar, benzaldehyde (0.47 mL, 4.06 mmol), pyrrole (0.56 mL, 8.12 mmol), and trifluoroacetic acid (20 µL, 0.26 mmol) were added. CH_2Cl_2 (300 mL) was added to the round bottom flask. The reaction was degassed with N_2 (g) for 20 min and was stirred at room temperature for 24 h under inert atmosphere. 2,3-Dichloro-5,6-dicyano-*p*-benzoquinone (920 mg, 4.06 mmol) suspended in CH_2Cl_2 (30 mL) was added under air and the mixture was allowed to stir for 30 min at room temperature. Triethylamine (7.90 mL, 56.8 mmol) and boron trifluoride diethyl etherate (8.12 mL, 65 mmol) were added and the reaction was left to stir for 24 h at room temperature. The reaction was diluted with H_2O (100 mL) and first extracted with CH_2Cl_2 (3 x 100 mL). The organic phases were combined, washed with brine (100 mL), dried over anhydrous Na_2SO_4 and filtered. The solvent was evaporated under reduced pressure. The crude mixture was purified by column chromatography [SiO_2:Hexanes/EtOAc 5:1 (v/v)] to yield the product (210 mg, 19%) as a dark red waxy solid. ^{1}H NMR (400 MHz, $CDCl_3$): δ 7.96 (2H, s), 7.51-7.62 (5H, m), 6.94-6.95 (2H, m), 6.54-6.55 (2H, m).^{13}C {^{1}H} NMR ($CDCl_3$, 400 MHz): δ 147.4, 144.1, 134.9, 133.8, 131.7, 130.8, 130.5, 128.5, 118.6. ^{11}B {^{1}H} NMR ($CDCl_3$, 400 MHz): δ 0.3 (t, J^{11}B -^{19}F = 28.3 Hz). ^{19}F {^{1}H} NMR ($CDCl_3$, 400 MHz): δ -145.3 to -145.0 (m, J ^{19}F -^{11}B = -28.8 Hz). EI-MS $[M]^+$ = 268.10 *m/z*.

1: N,N'-Difluoroboryl-5-(phenyl)dipyrrin (100 mg, 0.37 mmol) was added to a cleaned and oven-dried two-necked 100 mL round bottom flask equipped with a magnetic stir bar. The flask was attached to a reflux condenser and was put under a N_2 (g) atmosphere. In a separate 100 mL round bottom flask, a suspension of aluminum trichloride (75 mg, 0.56 mmol) in dry CH_2Cl_2 (10 mL) was prepared in a glovebox. The aluminum trichloride suspension was transferred under N_2 (g) to the two-necked flask. The mixture was refluxed under nitrogen at 40°C for 10 min. To a vial, catechol (100 mg, 0.91 mmol) was added and dissolved in CH_3CN (5 mL). The catechol solution was added dropwise under N_2 (g) to the reaction mixture. The reaction was allowed to cool down at room temperature and stir for 24 h, after which the solvent was evaporated under reduced pressure. The crude mixture was purified by column chromatography [SiO_2:Hexanes/CH_2Cl_2 1:3 (v/v)] to yield **1** (93 mg, 93%) as a red waxy solid. ^{1}H NMR (400 MHz, $CDCl_3$): δ 7.72 (2H, s), 7.52-7.62 (5H, m), 6.98 (2H, dd, J = 1.1, 4.2 Hz), 6.87-6.89 (2H, m), 6.80-6.82 (2H, m), 6.50 (2H, dd, J = 2.0, 4.3 Hz). ^{13}C {^{1}H} NMR ($CDCl_3$, 400 MHz): δ 150.9, 147.3, 145.1, 134.9, 133.8, 132.2, 130.8, 130.5, 128.5, 119.5, 118.9, 109.8. ^{11}B {^{1}H} NMR ($CDCl_3$, 400 MHz): δ 6.6 (s). EI-MS $[M]^+$ = 338.05 *m/z*.

3: To a cleaned and oven-dried 50 mL round bottom flask equipped with a magnetic stir bar, N-hydroxyphthalimide (1.00 g, 6.13 mmol) and *p*-toluenesulfonyl chloride (1.29 g, 6.74 mmol) were dissolved in THF (10 mL). Triethylamine (1.00 mL, 7.17 mmol) was added dropwise to the reaction mixture, which was then stirred at room temperature for 1 h. The solvent was evaporated under reduced pressure, after which 5% hydrochloric acid (15 mL) was added. The precipitate was filtered and washed with H_2O (2 x 15 mL). The solid was purified by recrystallization from ethyl acetate to yield **3** (1.27 g, 65%) as a white crystalline powder. ^{1}H NMR (400 MHz, $CDCl_3$): δ 7.95 (2H, dt, J = 1.8, 8.4 Hz), 7.83-7.86 (2H, m), 7.79-7.82 (2H, m), 7.39-7.41 (2H, m), 2.50 (3H, s). ^{13}C {^{1}H} NMR ($CDCl_3$, 400 MHz): δ 161.3, 147.1, 135.2, 130.8, 130.1, 129.6, 128.6, 124.3, 21.9.

4: To a mortar, *o*-nitrobenzyl alcohol (1.53 g, 10 mmol), *p*-toluenesulfonyl chloride (2.86 g, 15 mmol) and potassium carbonate (4.98 g, 36 mmol) were added. The solids were vigorously ground with a pestle for 5 min. Potassium hydroxide (2.81 g, 50 mmol) was added to the mixture and was ground for an additional 2 min in a fumehood. A highly exothermic reaction releasing HCl (g) occurred. The resultant brown paste was dissolved in Et_2O (50 mL) after which the solids were filtered and washed with Et_2O (3

x 10 mL). The organic filtrate was evaporated under reduced pressure. The solid was purified by recrystallization from hexanes to yield **4** (2.29 g, 74%) as brown crystals. ^{1}H NMR (400 MHz, $CDCl_3$): δ 8.13 (1H, dd, J = 1.3, 8.2 Hz), 7.85 (2H, dt, J = 2.0, 8.4 Hz), 7.76-7.78 (1H, m), 7.69 (1H, td, J = 1.3, 7.5 Hz), 7.49-7.53 (1H, m), 7.36-7.38 (2H, m), 5.48 (2H, s), 2.46 (3H, s). ^{13}C {^{1}H} NMR ($CDCl_3$, 400 MHz): δ 146.7, 145.3, 134.2, 132.6, 130.5, 130.1, 129.2, 128.9, 128.0, 125.1, 68.1, 21.7.

Silver Nanostructures (AgNP): AgNP were prepared according to a modified version of our previously published protocol.[S2c] To a clean, oven dried 50 mL Erlenmeyer flask, 34.4 mL of MilliΩ H_2O, 4.0 mL of 10 mM trisodium citrate, 0.80 mL of 10 mM I-2959 and 0.8 mL of 10 mM $AgNO_3$ solutions were added. The mixture was degassed with N_2 for 30 min, after which it was irradiated at 365 nm for 10 min in a Luzchem LCZ-4 photoreactor (14 bulbs, 100 W/m^2). The dark yellow silver seed solution was then gently oxygenated for 40 min and irradiated for 18 h with four 590 nm LEDs (700 mA, 3.3 W per LED) to yield a dark blue solution of triangular silver nanoplates. The nanoplates were transferred into two 50 mL tubes (Cell Treat) and centrifuged at 15°C for 20 min at 14,000 rpm. The supernatants were discarded, and the remaining pellets were combined and resuspended in MilliΩ H_2O (4 mL).

Methods

Chemicals were purchased from Sigma-Aldrich, Fisher Scientific and ACP Chemicals. Solvents were purchased from ACP Chemicals. Dry CH_2Cl_2 was purified with a MBraun MBM-SPS solvent purification system. Ultrapure deionized water (MilliΩ, 18.2 MΩ) was obtained from a Millipore Purification System. All the reactions were monitored by thin-layer chromatography, using aluminium sheets coated with silica (60, F_{254}). Column chromatography was performed using SiliaFlash® P60, 40-63 μm (230-400 mesh) silica gel. NMR spectra were recorded at room temperature with a Bruker Avance 400 spectrometer. Mass spectral analysis was performed with a 7890B GC System equipped with a 5977 mass selective detector from Agilent Technologies. Steady-state absorption spectra were recorded with an Agilent Cary 60 UV-visible spectrophotometer, using quartz cells with a path length of 1 cm. Steady-state emission spectra were recorded with an Agilent Cary Eclipse spectrofluorimeter in aerated solutions. Diffuse reflectance spectroscopy was performed using an Agilent Cary 5000 UV-visible spectrophotometer equipped with an internal diffuse reflectance accessory (DRA-2500). Illumination at 254 nm was performed with a Luzchem LCZ-4 photoreactor equipped with 6 UVC bulbs (8 W each). This UVC source did not provide efficient activation of **4** or **6**. Illumination at 365 nm was performed using an in-house designed illumination setup consisting of a set of up to four light-emitting diodes (LEDs, LEDEngin LZ4-UV00) each connected to a heat sink and diaphragm-based active cooling system (Nuventix SynJet). A DC Power Supply provided a current of 700 mA. According to manufacturer specifications these conditions deliver an average radiant flux of 3.3 W per LED. Solutions were irradiated with four LEDs while films only required one LED. For solution experiments, 2.9 mL of a 10 μM stock solution of **1** in MeOH and 0.1 mL of 3 mM (10 equivalents) stock solutions of PTSA or PAGs in MeOH were mixed and used immediately. For the preparation of thin polymer films, 3.17 mg of **3** or 3.07 mg of **4** (20 equivalents) were added to 1 mL of a 500 μM stock solution of **1** in 20% (w/v) polyvinylpyrrolidone (PVP, 55 kDa) in MeOH and sonicated until completely dissolved. The mixtures were spin coated on glass slides (Fisher Scientific) at 1000 rpm for 40 s. The coated slides were used immediately. The same protocol was employed to deposit polymer films on glass slides pre-coated with silver nanoparticles. Brownian motion was partially restricted by the increased viscosity of the polymer film relative to experiments in solution, but any fluorophore motion was still random and without AgNP specificity. SEM images were recorded with a Hitachi S-5200 operating at 5.0 kV acceleration voltage. Samples for electron microscopy were prepared by drop casting a dilute solution of AgNP onto carbon square mesh copper TEM grids (Electron Microscopy Sciences, CF400-CU-UL) before drying overnight under ambient conditions or reduced pressure.

Single-Molecule Fluorescence Microscopy

Single molecule experiments were conducted on an instrumental setup comprising an Andor Diskovery multi-modal imaging system (TIRFM, confocal, brightfield, epifluorescence) by Quorum Technologies Inc., coupled to a Leica DMi8 inverted microscope. For TIRFM and brightfield microscopy utilized in this study, a 63× oil immersion objective (NA 1.49) and 1.8× camera relay provided a total of 108× magnification. For TIRFM, samples were excited using a 488 nm direct modulation laser source from an Andor Integrated Laser Engine, operating at 10% power. Note that nanoparticle blinking is not a concern at the low irradiance used here for TIRFM.[S1] After excitation light passed through the objective and impinged upon the sample, a portion was reflected back through the objective along with fluorescence emission and passed through a 50 nm band pass emission filter centred at 525 nm before being collected by an Andor iXon 897 EMCCD camera. For TIRFM, the EM Gain was set to 100, the TIRF depth was set to 500 nm (effectively setting the TIRF angle), and exposure time was 50 ms (i.e. image sequences were recorded at 20 frames/s). For brightfield microscopy, the EM gain was reduced to 3 and exposure time was 5 ms. In both cases, Quorum Wave FX acquisition software (powered by MetaMorph) was used to control instrument parameters and to obtain images consisting of 512 × 512 pixels (px) at a scale of 153 nm/pixel, for a total image area of 78.14 μm × 78.14 μm (6105.86 μm^2).

Samples for single molecule experiments were prepared in manner analogous to macroscale PVP thin films, with the exception that 0.17 mm #1.5 glass coverslips (Fisher Scientific), the optimal thickness for TIRFM, were used as the sample substrate. Concentrated AgNP were drop casted onto coverslips to cover approximately half the substrate area and were dried overnight under ambient conditions prior to the preparation of doped PVP films. The latter were prepared by spin coating a methanolic solution of **1** (100 nM), **4** (2 μM, 20 equiv.) and 20% PVP (55 kDa). All samples were transported in the dark and used immediately. During single molecule microscopy experiments, *in situ* UVA irradiation of samples was accomplished using 365 nm light (0.4 mW cm^{-2}) from a laboratory TLC lamp (Mineralight UVGL-25). In addition to a sample thickness, AgNP-fluorophore distance was restricted by the penetration depth of the TIRF evanescent field, which decays exponentially in the axial direction (orthogonal to the sample surface) and is typically diminished at a maximum distance of 100 nm for shorter excitation wavelengths such as 488 nm and low laser power used here. At longer excitation wavelengths and higher laser power, the field may extend to 200 nm or more.

Image analysis was performed using a combination of Fiji (ImageJ), MatLab, OriginPro and Microsoft Excel software, based on modified literature protocols.[S2] In brief, raw TIRF image sequences were imported into Fiji, where background subtraction was consistently performed using a 10 px rolling ball algorithm (brightfield images were not adjusted). From here, videos were analysed using an in-house written MatLab protocol which builds upon the well-established LocalizerMatlab.mex64 script developed by Peter Dedecker (University of Luven, Belgium)[S3] for the localization of single molecule fluorescence bursting in super-resolution microscopy. Essentially, our algorithm conducts a frame by frame analysis of TIRF image sequences using a Generalized Likelihood Ratio Test (GLRT) to categorize relative pixel intensity fluctuations and fit them to a 2D Gaussian approximation of the Point Spread Function describing fluorophore emission. The algorithm then filters the results to remove duplication and returns the xy coordinates (in pixel units) of potential emitters. Next, these locations were used as the centre points for circular, 1.5 px radius regions of interest (ROIs), automatically generated and imported into the Fiji ROI manager tool using an in-house written macro. From here, Fiji was used to map the cumulative mean intensity of each pixel across 1000 frames (i.e. 3D surface projection) and to measure the mean intensity within each ROI for each frame individually. These data were utilized to plot intensity-time trajectories and perform statistical analysis of fluorescence bursting events using OriginPro and MS Excel. Burst intensities for individual intensity-time trajectories were taken as the difference between peak intensity and baseline signal.

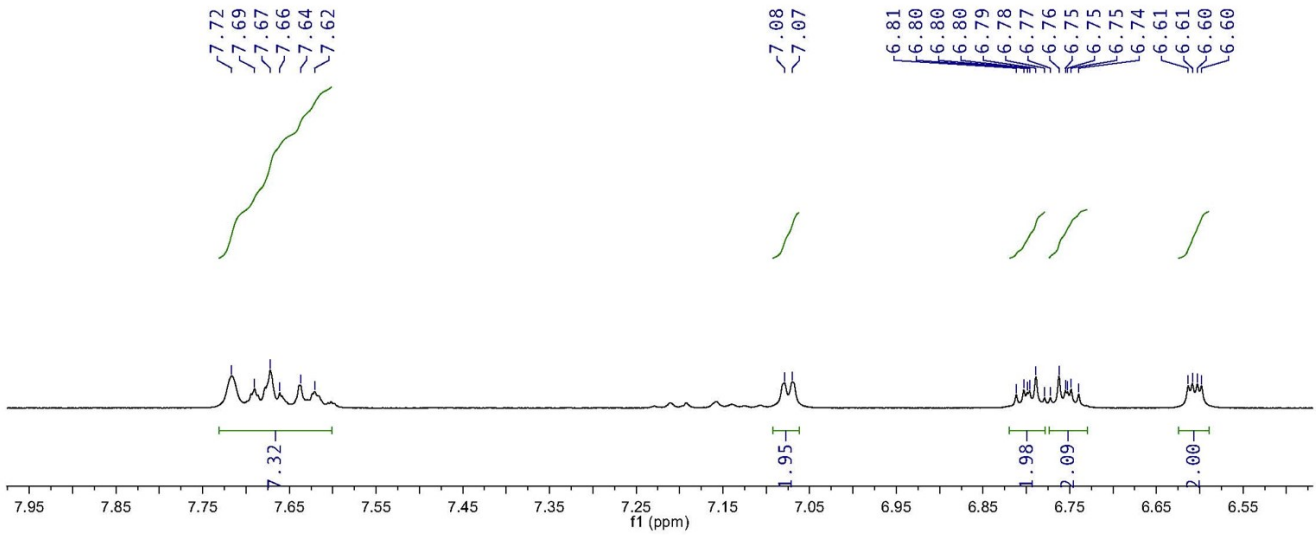

Figure S1. ^{1}H NMR spectrum (400 MHz) of a CD_3OD solution (15 mM, 20°C) of **1**.

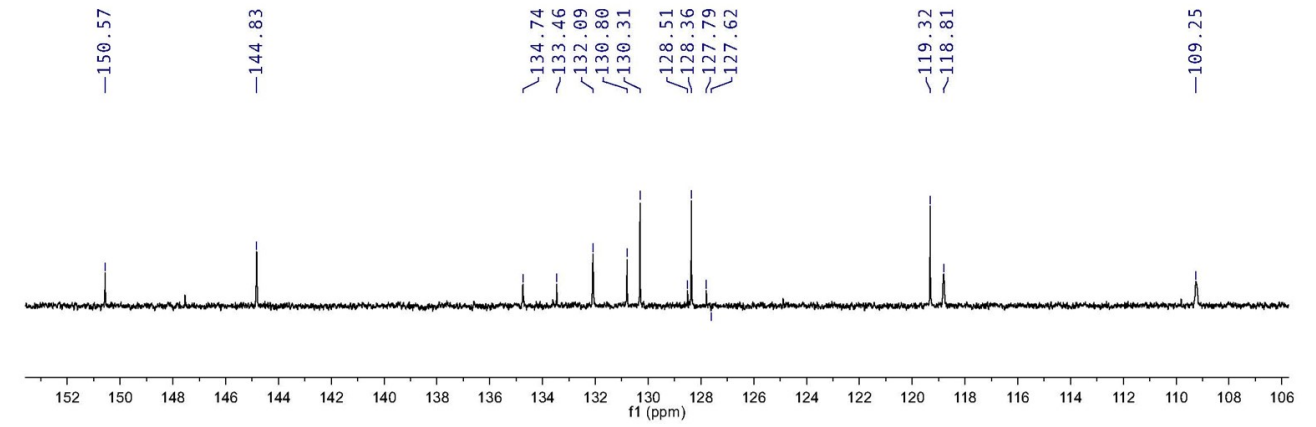

Figure S2. ^{13}C $\{^{1}H\}$ NMR spectrum (400 MHz) of a CD_3OD solution (15 mM, 20°C) of **1**.

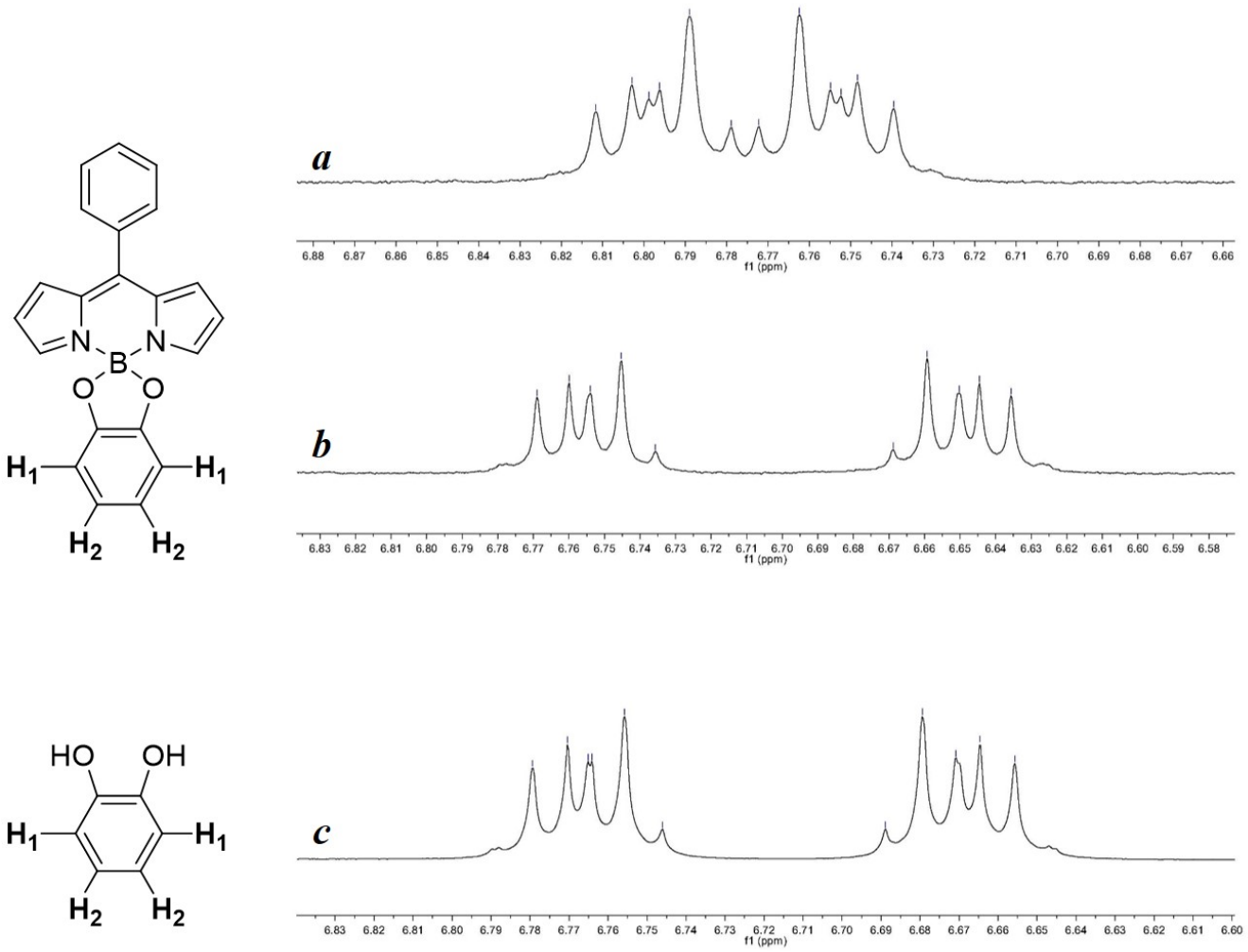

Figure S3. ^{1}H NMR spectra (400 MHz) of a CD_3OD solution (15 mM, 20°C) of **1** before (***a***) and 4 hours after (***b***) the addition of 10 equivalents of PTSA, and of catechol (***c***).

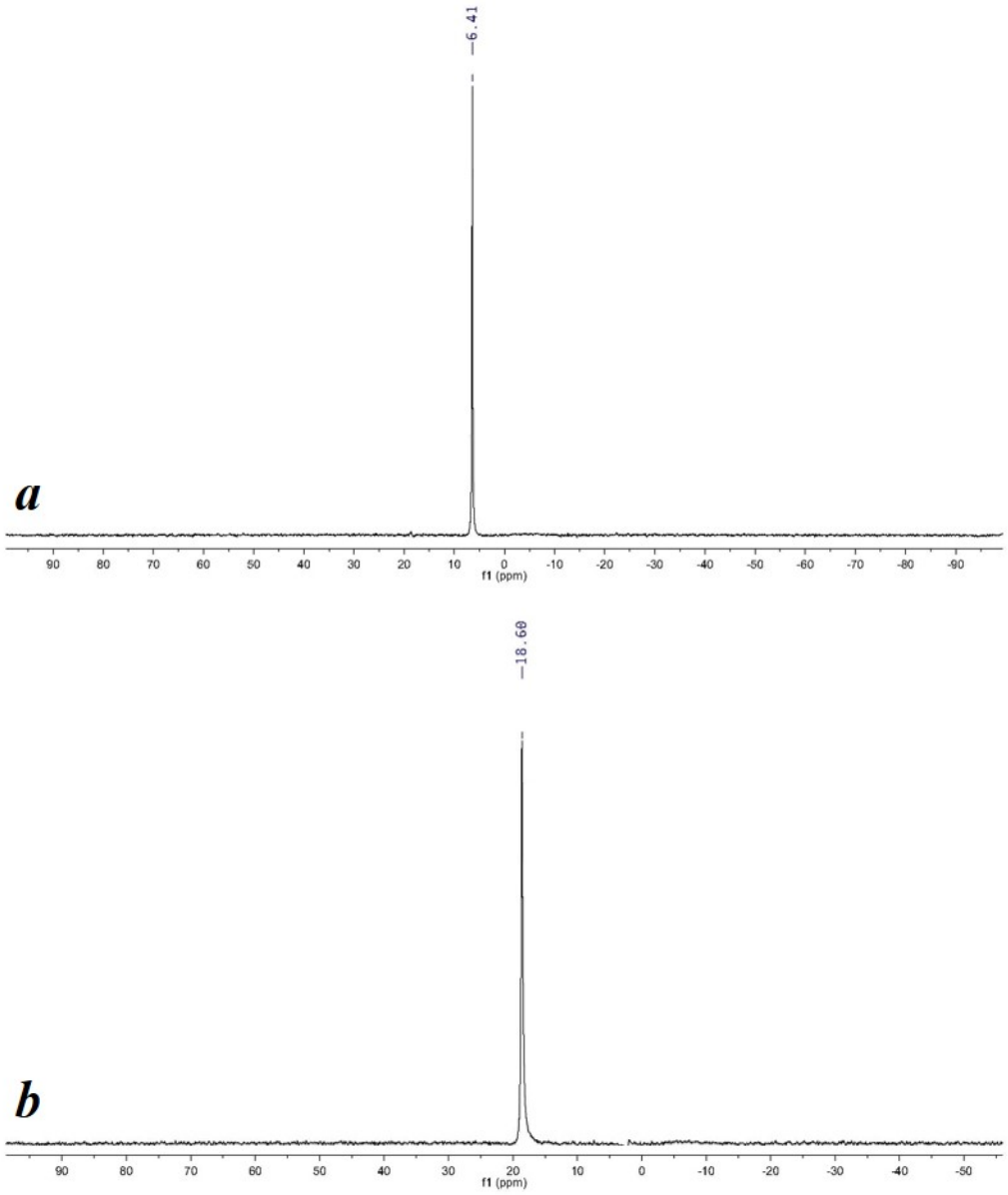

Figure S4. ^{11}B $\{^{1}H\}$ NMR spectra (400 MHz) of a CD_3OD solution (15 mM, 20°C) of **1** before (***a***) and 4 hours after (***b***) the addition of 10 equivalents of PTSA.

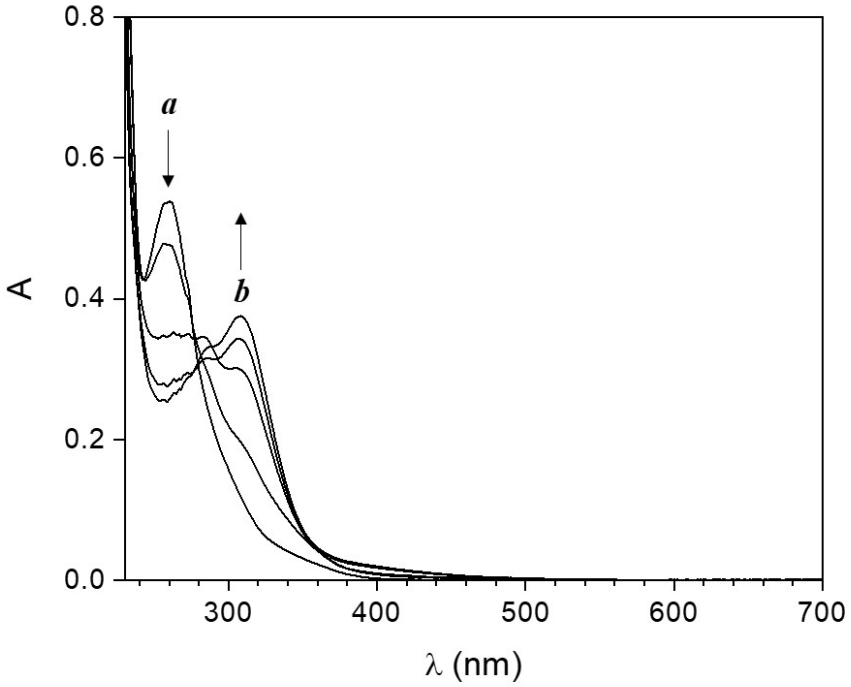

Figure S5. Absorption spectra of a solution (100 μM, MeOH, 20°C) of **4** recorded before and after irradiation (365 nm, 0-20 min).

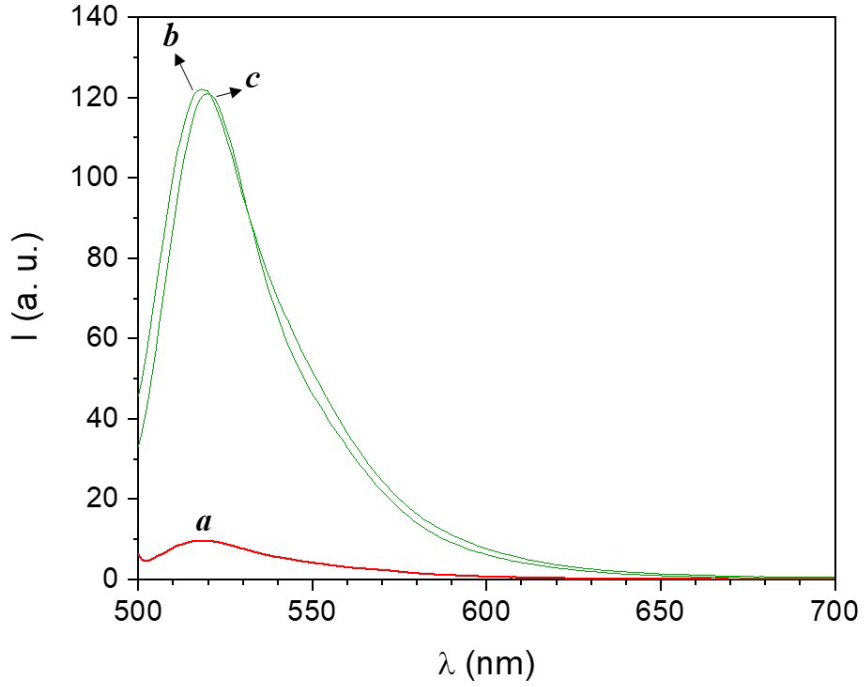

Figure S6. Emission spectra of a solution of **1** (10 μM, 20°C, λ_{Ex} = 490 nm) before (***a***) and after (***b*** and ***c***) UVA (***b***, 365 nm, 20 min) or UVC (***c***, 254 nm, 20 min) irradiation.

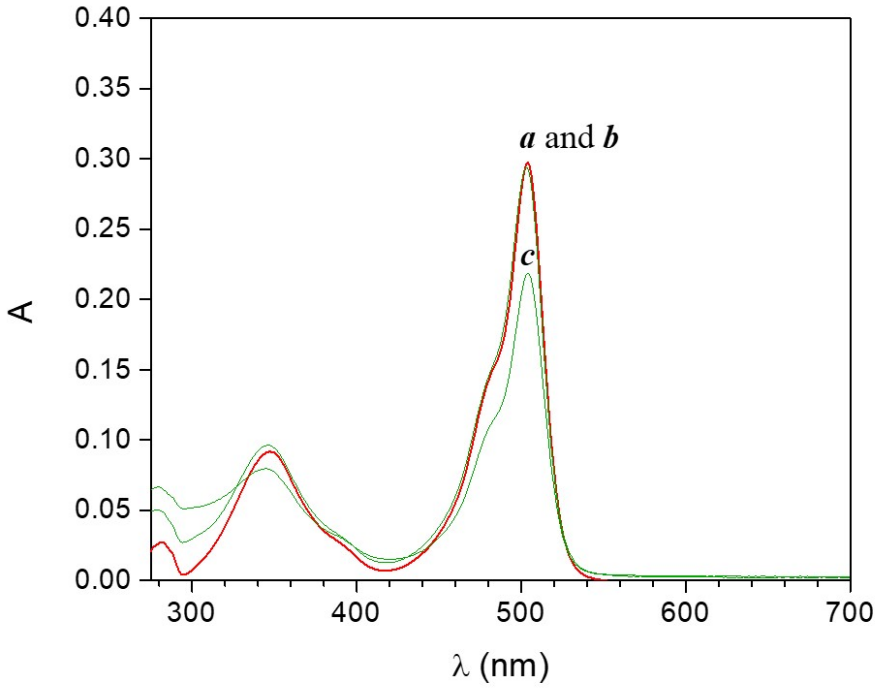

Figure S7. Absorption spectra of a solution of **1** (10 μM, 20°C) before (***a***) and after (***b*** and ***c***) UVA (***b***, 365 nm, 20 min) or UVC (***c***, 254 nm, 20 min) irradiation.

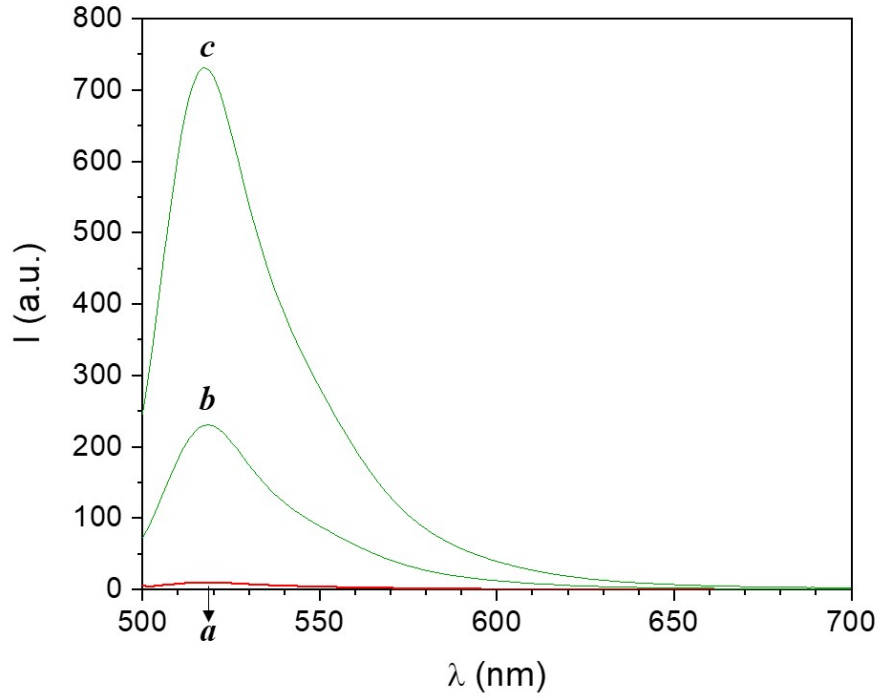

Figure S8. Emission spectra of a solution of **1** (10 μM, 20°C, λ_{Ex} = 490 nm) and **5** (100 μM, ***a*** and ***b***) before (***a***) and after (***b***) UVC (254 nm, 20 min) irradiation. Emission spectra of a solution of **1** (10 μM, 20°C, λ_{Ex} = 490 nm) and **6** (100 μM, ***a*** and ***c***) before (***a***) and after (***c***) UVA (365 nm, 20 min) irradiation.

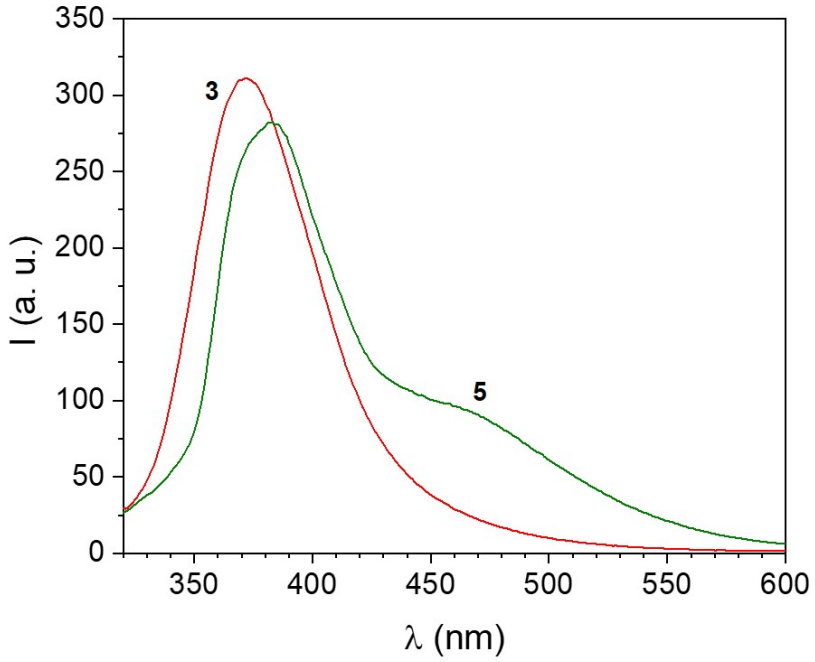

Compound	Integrated Fluorescence Intensity
3	21998.34508
5	26525.94078

Figure S9. Emission spectra of solutions of **3** and **5** in CH_3OH, having matched absorbance below 0.1 at the excitation wavelength of 308 nm. Notice that under these conditions, the higher integrated fluorescence intensity of **5** indicates a higher quantum yield of fluorescence. It follows that the competition between radiative relaxation and photoacid generation is more heavily weighted toward the latter for compound **3** vs. **5**.

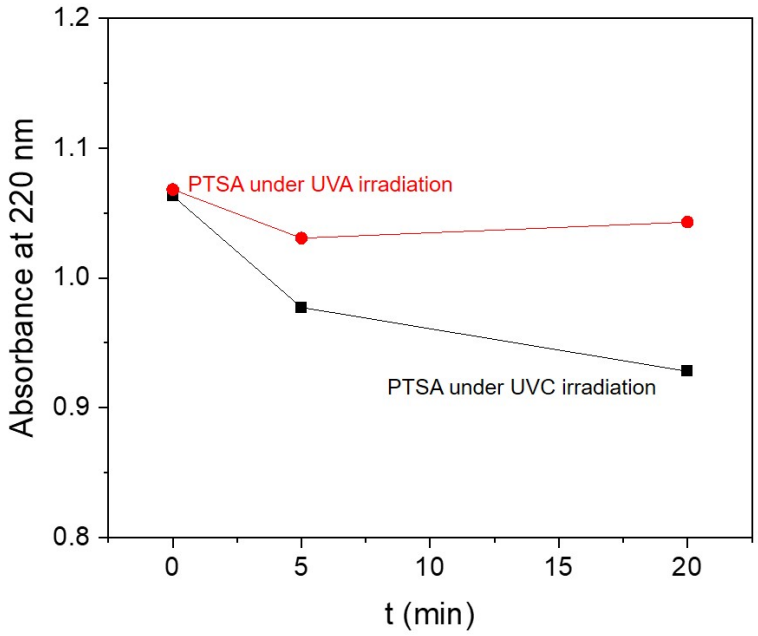

Figure S10. Absorption at 220 nm of a solution of PTSA (100 μM, 20°C) under UVA (365 nm) or UVC (254 nm) irradiation.

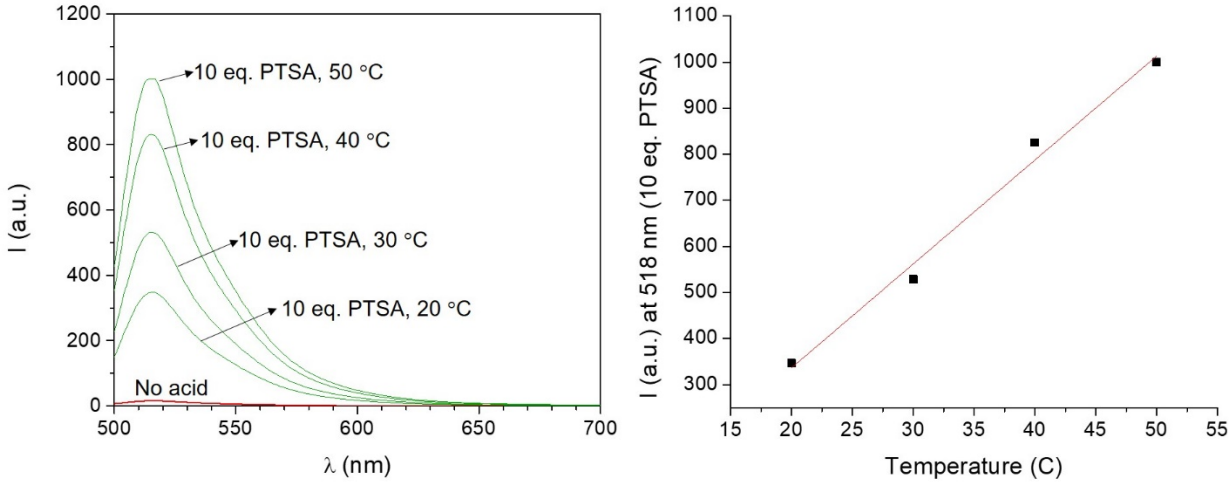

Figure S11. Fluorescence spectra and emission maxima of a solution of **1** (10 μM, λ_{Ex} = 490 nm) and PTSA (100 μM) in a thermal bath (20 to 50°C).

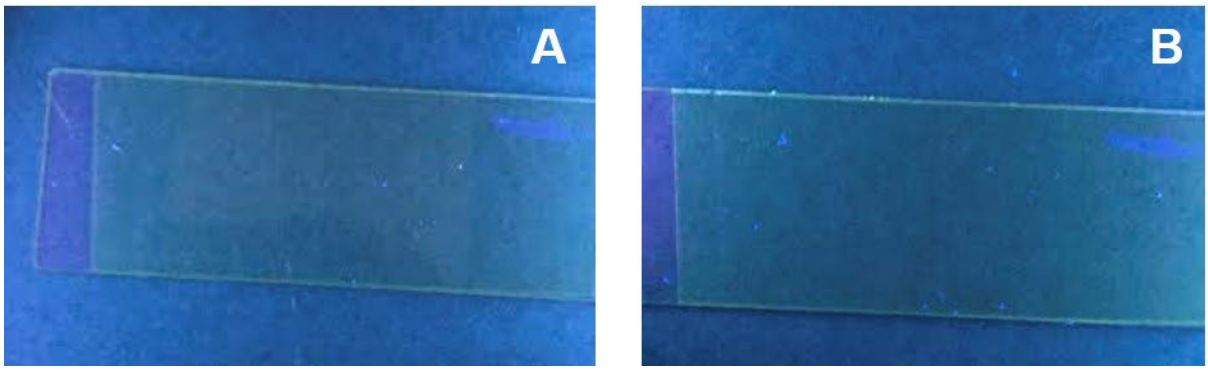

Figure S12. Photographs of a thin PVP (55 kDa, 20% w/v in MeOH) film containing **1** (500 μM) before (***a***) and after (***b***) after exposure at 254 nm for 20 min through a 3D printed mask.

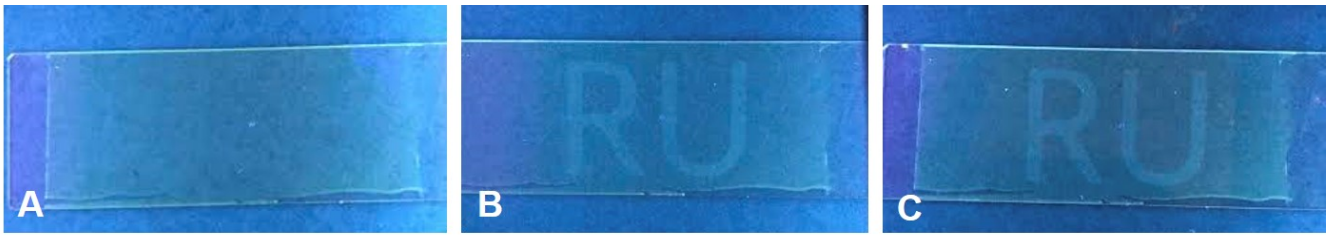

Figure S13. Photographs of a thin PVP (55 kDa, 20% w/v in MeOH) film containing **1** (500 μM) and **4** (10 mM) before (***a***), immediately after (***b***) and 10 minutes after (***c***) exposure at 365 nm for 60 min through a 3D printed mask.

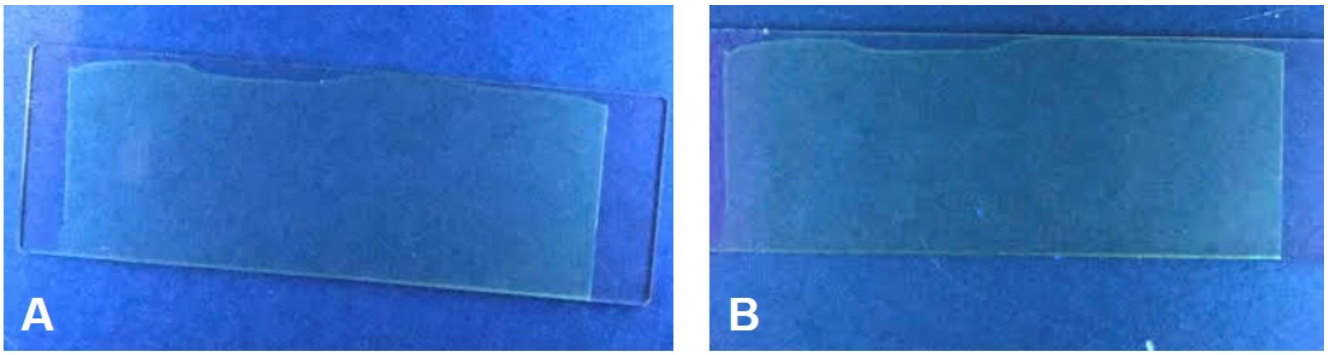

Figure S14. Photographs of a thin PVP (55 kDa, 20% w/v in MeOH) film containing **1** (500 μM) before (***a***) and after (***b***) after exposure at 365 nm for 60 min through a 3D printed mask.

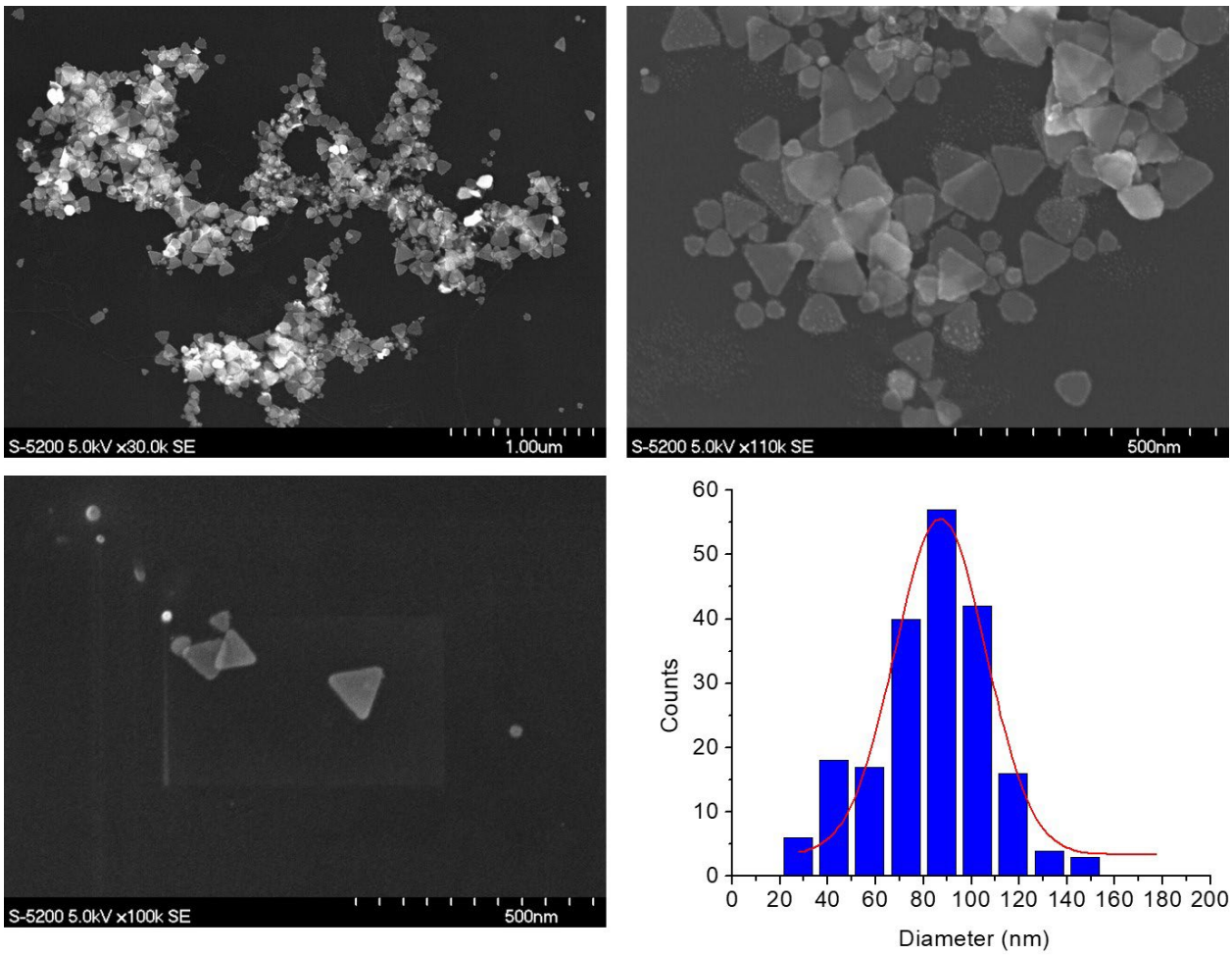

Figure S15. Scanning Electron Microscopy (SEM) of AgNP. Histogram showing Gaussian distribution of AgNP diameters measured using spherical particle approximation in Fiji (ImageJ).

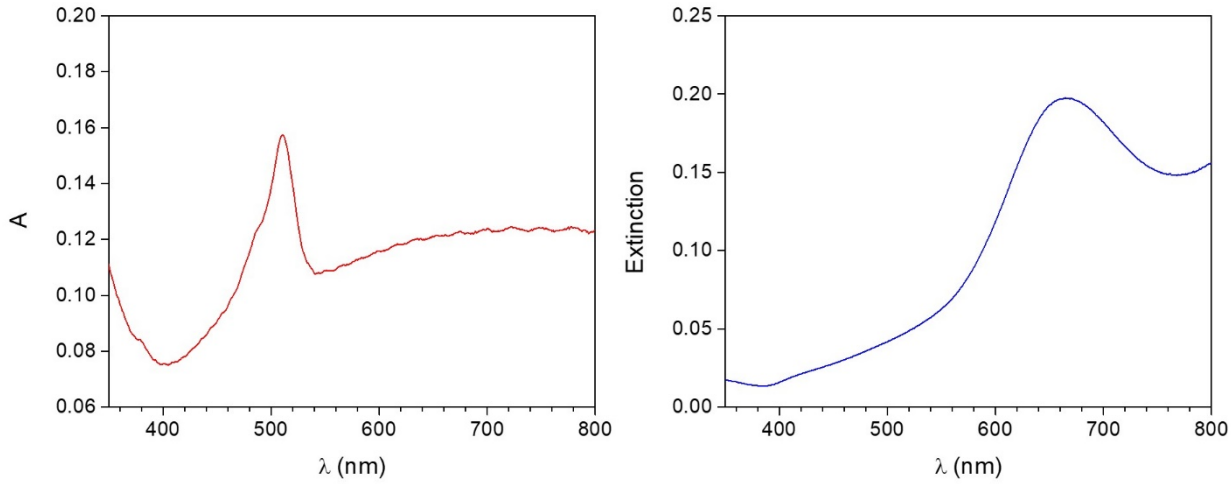

Figure S16. ***Left:*** Absorption spectrum of a PVP (55 kDa, 20% w/v in MeOH) film containing **1** (500 μM) atop AgNP. ***Right:*** Extinction spectrum of AgNP in MilliΩ H_2O.

Thin Film Thickness and Maximum AgNP-Fluorophore Distance

The thickness d of a thin PVP film spin-coated onto a glass microscope slide as described on page S3 was estimated upon the basis of thin film interference.[S4] A portion of light incident normal to the sample surface experiences a phase shift φ_1 equivalent to one half wavelength upon specular reflectance at the air/polymer interface (location 1 in the diagram below), where the index of refraction of air n_{air} is less than that of the polymer n_{PVP} (*vide infra*). The remaining light penetrates the film and slows down as it moves through the polymer. It is reflected at the polymer/glass interface (location 2 below) and emerges from the material having traveled an extra distance $2d$ relative to the light reflected at location 1.

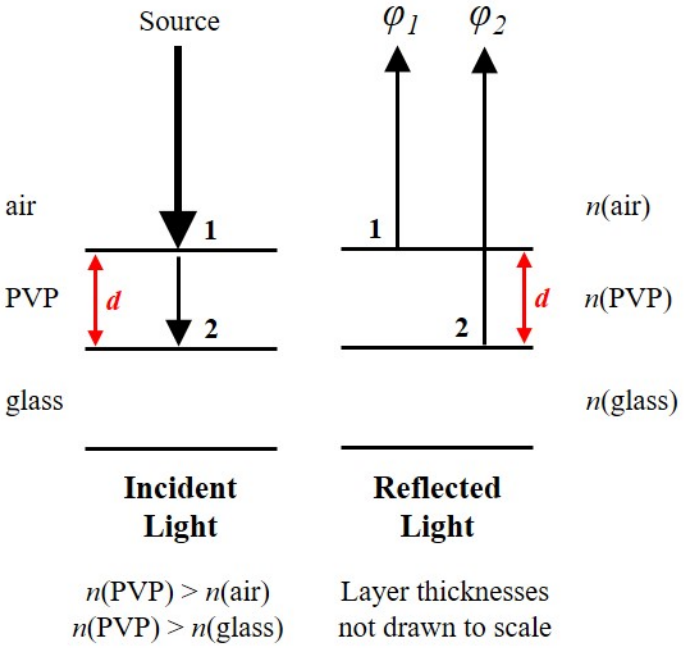

Since $n_{PVP} > n_{glass}$ (*vide infra*) specular reflectance at location 2 induces a phase shift φ_2 of $2d$. The relative phase shift Φ between the two spectrally reflected waves is thus;

$$\Phi = \varphi_2 - \varphi_1$$

$$\Phi = 2d - \frac{\lambda_{PVP}}{2}$$

The two traveling waves are moving in the same direction and can interfere constructively or destructively with one another. To determine which type of interference occurs, UV-visible spectroscopy was used to obtain the specular reflectance of the sample as a function of wavelength (Figure S17). This was done by subtracting the diffuse reflectance spectrum of the sample from its total reflectance spectrum, assuming a flat sample of uniform thickness. As shown in Figure S17, specular reflectance is higher for the PVP film relative to the glass substrate all across the UV-visible region, indicative of partial constructive interference between the two waves reflected at locations 1 and 2. The relative phase shift Φ can therefore be set equal to the condition for constructive interference as follows;

$$m\lambda_{PVP} = \Phi = 2d - \frac{\lambda_{PVP}}{2}$$

Which can be rearranged to;

$$2d = \lambda_{PVP}\left(m + \frac{1}{2}\right)$$

where *m* is an integer (0, 1, 2…) corresponding to the periodic nature of interference patterns. Complete constructive interference occurs wherever the path length between two waves differs by an integer multiple of wavelengths. The dominant interference fringe is of the zeroth order, hence *m* is set equal to zero here. The relationship between wavelength in the polymer (where the difference in path length occurs) and wavelength measured in air by UV-visible spectroscopy is;

$$\lambda_{PVP} = \frac{\lambda_{air}}{n_{PVP}}$$

Substituting for λ_{PVP} and isolating the film thickness *d*, we arrive at;

$$d = \frac{\lambda_{air}}{4n_{PVP}}$$

As shown in Figure S17, the dominant wavelengths of specular reflectance are 360 and 400 nm, with a shoulder centred at 500 nm.

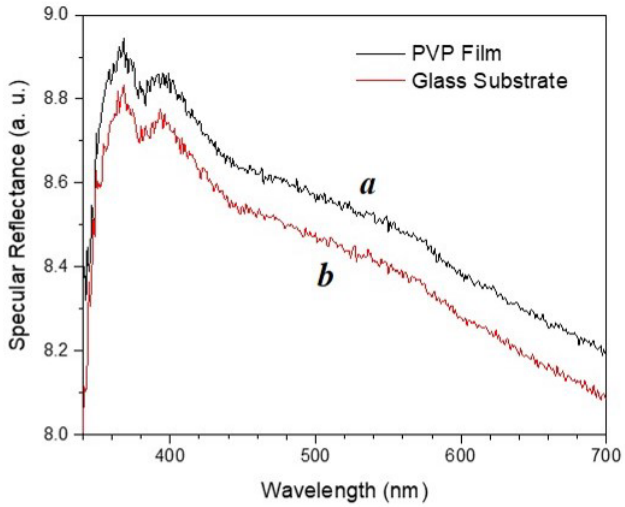

Figure S17. Specular reflectance as a function of wavelength for (***a***) a thin PVP film and (***b***) the bare glass substrate.

The index of refraction of the polymer can be computed at each wavelength according the following expression from the literature, where the wavelength unit is micrometers:[S5]

$$n_{PVP} = 1.5151 + \frac{0.00279}{\lambda^2} + \frac{5.0756 \times 10^{-4}}{\lambda^4}$$

Wavelength (μm)	Index of Refraction
0.360	1.5668
0.400	1.5524
0.500	1.5344

As shown above, the tabulated indices of refraction for PVP are indeed higher than those of air (1.0003) and glass (1.5000) at all three wavelengths.[S4] The PVP film thickness range can therefore be estimated as follows;

Using 360 nm;

$$d = \frac{\lambda_{air}}{4n_{PVP}} = \frac{360\text{ nm}}{4(1.5668)} = 57.44 = 57\text{ nm}$$

Using 400 nm;

$$d = \frac{\lambda_{air}}{4n_{PVP}} = \frac{400\text{ nm}}{4(1.5524)} = 64.42 = 64\text{ nm}$$

Using 500 nm;

$$d = \frac{\lambda_{air}}{4n_{PVP}} = \frac{500\text{ nm}}{4(1.5344)} = 81.47 = 82\text{ nm}$$

It follows that the PVP film thickness is approximately 57–82 nm when prepared according to the reported spin coating conditions in the absence of AgNP. Not only would the presence of AgNP have impacted specular reflectance measurements, the thickness of the PVP layer is more important than the total sample thickness because we are more interested in determining the maximum possible distance between AgNP and fluorophores distributed throughout the PVP matrix, which can evidently be as high as about 82 nm. Previous research has shown that preparing such films atop glass slides coated with these same AgNP caused the total sample thickness to increase by 22 ± 5 nm, for a total sample thickness in the range of 74–109 nm, or roughly 100 nm.[S2c]

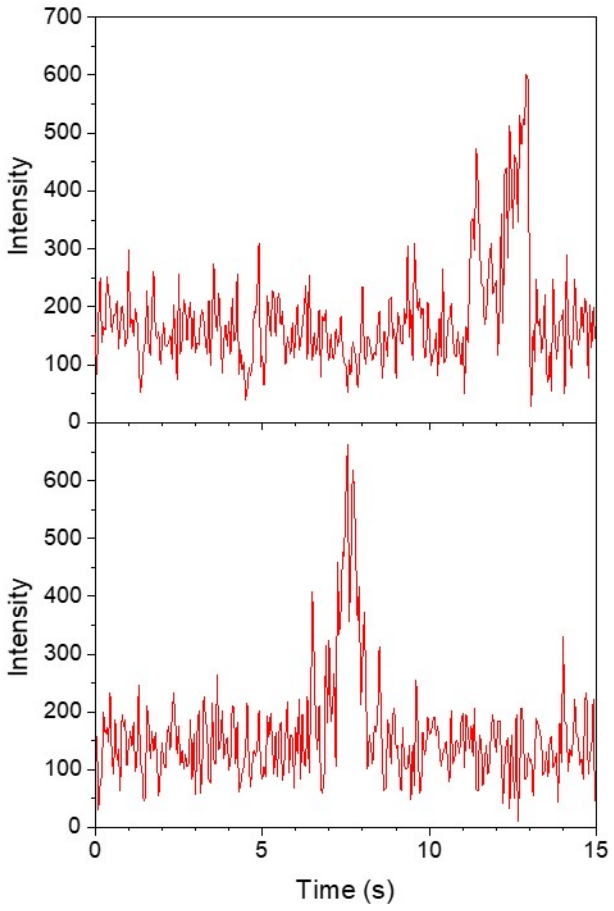

Figure S18. Representative single molecule fluorescence intensity-time trajectories in the absence of AgNP after 1 min irradiation at 365 nm.

References

S1 C. D. Geddes, A. Parfenov, I. Gryczynski and J. R. Lakowicz, *J. Phys. Chem. B,* 2003, **107**, 9989.

S2 a) G. K. Hodgson, S. Impellizzeri and J. C. Scaiano, *Chem. Sci.,* 2016, **7**, 1314; b) G. K. Hodgson, S. Impellizzeri and J. C. Scaiano, *Catal. Sci. Technol*., 2016, **6**, 7113; c) S. Impellizzeri, S. Simoncelli, G. K. Hodgson, A. E. Lanterna, C. D. McTiernan, F. M. Raymo, P. F. Aramendia and J. C. Scaiano, *Chem. Eur. J.*, 2016, **22**, 7281.

S3 P. Dedecker, S. Duwe, R. K. Neely and J. Zhang, *J. Biomed. Opt*., 2012, **17**, 126008.

S4 R. D. Knight, *Physics for Scientists and Engineers: A Strategic Approach*, Pearson, San Francisco, 2004, pp. 632-692.

S5 T. A. Konig, P. A. Ledin, J. Kerszulis, M. A. Mahmoud, M. A. El-Sayed, J. R. Reynolds and V. V. Tsukruk, *ACS Nano*, 2014, **8**, 6182.